

Time-Resolved Dynamics in N_2O_4 Probed Using High Harmonic Generation

Wen Li,^{1*} Xibin Zhou,¹ Robynne Lock,¹ Serguei Patchkovskii,² Albert Stolow,² Henry C. Kapteyn,¹ Margaret M. Murnane¹

The attosecond time-scale electron-recollision process that underlies high harmonic generation has uncovered extremely rapid electronic dynamics in atoms and diatomics. We showed that high harmonic generation can reveal coupled electronic and nuclear dynamics in polyatomic molecules. By exciting large amplitude vibrations in dinitrogen tetroxide, we showed that tunnel ionization accesses the ground state of the ion at the outer turning point of the vibration but populates the first excited state at the inner turning point. This state-switching mechanism is manifested as bursts of high harmonic light that is emitted mostly at the outer turning point. Theoretical calculations attribute the large modulation to suppressed emission from the first excited state of the ion. More broadly, these results show that high harmonic generation and strong-field ionization in polyatomic molecules undergoing bonding or configurational changes involve the participation of multiple molecular orbitals.

In polyatomic molecules, electronic and vibrational excitations can couple and rapidly redistribute both energy and charge during dynamic processes. Because of the importance of these dynamics in chemical and biological systems, the ability to probe dynamics in larger polyatomic molecules ultimately is a requirement for any broadly useful spectroscopy or dynamical imaging technique. As an example, time-resolved photoelectron spectroscopy (TRPES) is a weak-field perturbative method that can probe these dynamics (1–3). In TRPES, the molecule is first excited by a pump pulse. A time-delayed probe pulse then projects the complex evolving wave packet onto the molecular ionization continuum, and the outgoing electron is analyzed as a function of pump-probe delay. The cation electronic states, their associated electronic continua, and the vibrational structure of the ionization continuum are used as “templates” for projecting out the electronic and vibrational components of the complex wave packet. This evolving projection onto multiple electronic continua permits the disentangling of electronic and vibrational dynamics during nonadiabatic processes in polyatomic molecules (4).

High harmonic generation (HHG) is a strong-field nonperturbative process (5, 6) that is closely related to photoelectron spectroscopy, occurring at laser intensities of $>10^{13}$ W cm⁻². In atoms, HHG is successfully described by an adiabatic single active electron (SAE) model involving three steps: strong-field tunnel ionization, propagation of the continuum electron in response to

the laser field, and finally, recombination of the electron with its parent ion, which results in the emission of a high-energy photon (7–10). However, in the case of HHG from a polyatomic molecule, the physics is more complex because of the many-body electronic structure of polyatomic molecules and the existence of rovibrational and nonadiabatic dynamics. The recombination matrix element for the HHG process and the photoionization matrix element of the photoabsorption process are the same because these steps are the inverse of each other. Therefore, the multiple electronic continua relevant to probing complex polyatomic dynamics via TRPES must also play a role when HHG is used to probe these dynamics. The use of HHG as a probe has two potential advantages over TRPES: the ability to access attosecond-time-scale processes and the ability of HHG to simultaneously probe with many photon energies. However, until recently (11, 12), only the highest occupied molecular orbital (HOMO) has usually been considered to explain both strong-field ionization and high harmonic emission. This simplification comes from the adiabatic and SAE approximations that underlie theories of tunnel ionization in atoms and molecules [Ammosov-Delone-Krainov (ADK) and molecular ADK (13, 14) models] and are integral to the three-step model of HHG (7–9). In polyatomic molecules, however, both approximations can fail dramatically, particularly so when the molecule is dynamically evolving, as we show here. Strong-field ionization can become nonadiabatic and involve multielectron excitations (15, 16). Theoretical efforts to relax the SAE approximation are being attempted in order to address these issues by introducing multielectron effects in the recombination step of HHG (11, 12, 17, 18).

Prior investigations showed that HHG from rotational axis-aligned molecules is a potential

probe of static molecular structure (19, 20) because the emission strength depends on the molecular orbital nature of the ground electronic state and its alignment with respect to the laser field. Recent related work used the photoelectrons released and rescattered during the strong-field ionization process to recover the static orbital structure of simple diatomic molecules (21). HHG was also used as a probe of simple dynamics in molecules in which, for example, the molecular structure varied slightly without any bond reorganization. Past work showed that the HHG process is sensitive to simple vibrational dynamics in a molecule, even to modes that cannot readily be optically probed (22, 23). The rearrangement of atoms within a molecule during the HHG process can also be inferred by comparing HHG spectra of isotope-substituted molecules (24). Chemical dynamics, however, involve large-amplitude motions. HHG experiments have yet to succeed in observing and understanding large-amplitude structural rearrangements within a polyatomic molecule, in which the simple assumptions are unlikely to remain valid because of dramatic and evolving changes in the ionization/recombination dynamics.

We successfully applied HHG as a time-resolved probe of chemical dynamics in a polyatomic molecule. By exciting a large-amplitude vibrational wave-packet motion in the ground state of a dinitrogen tetroxide (N_2O_4) molecule, we observed large modulations in harmonic yield. We discovered that at the outer turning point of the vibration, tunnel ionization populates the ground state of the ion ($\text{HOMO}^+ \text{A}_g$ continuum), which has a large recombination dipole and therefore a high probability for harmonic emission. In contrast, at the inner turning point, the first excited state of the ion is populated by tunnel ionization [that is, the $(\text{HOMO}-1)^+ \text{B}_{2g}$ continuum]. This channel has a reduced recombination cross-section and thus suppresses the harmonic emission.

HHG probing of N_2O_4 dynamics. N_2O_4 is a dimer of NO_2 , with a dissociation energy of ~ 0.65 eV. N_2O_4 can be present in dominant quantities (80%) even at room temperature. The molecule has D_{2h} symmetry and six Raman-active vibrational modes, the strongest being the low-frequency N-N symmetric stretch (265 cm⁻¹, 0.03 eV). By nonresonantly exciting this mode via impulsive stimulated Raman scattering (ISRS), we were able to generate a large-amplitude ground-state vibrational wave packet along the N-N coordinate. This large-amplitude motion correlates upon ionization with a broad range of ionic configurations, leading to the participation of more than one molecular ionization continuum in the HHG process (Fig. 1).

In our experiment, ultrashort laser pulses from a Ti:sapphire laser system (800 nm, ~ 30 fs, 4 mJ, and 1 kHz) were split into pump and

¹JILA and Department of Physics, University of Colorado and National Institute of Standards and Technology, Boulder, CO 80309-0440, USA. ²Steele Institute for Molecular Sciences, National Research Council, Ottawa, ON K1A 0R6, Canada.

*To whom correspondence should be addressed. E-mail: wli@jila.colorado.edu

probe pulses. The pump pulse was focused onto a N_2O_4 gas jet (backing pressure ~ 700 torr) at an incident intensity of $\sim 2 \times 10^{13} \text{ W cm}^{-2}$ to impulsively excite ground-state vibrations in the molecule. The time-delayed probe pulse was focused to an intensity of $\sim 2 \times 10^{14} \text{ W cm}^{-2}$ to generate high harmonics from the vibrationally excited molecules. The relative polarizations of the pump and the probe pulses were controlled using a half-wave plate in the pump-beam path. The generated harmonics were then spectrally separated using an extreme ultraviolet (EUV) spectrometer and imaged onto an EUV-sensitive charge-coupled device camera (Andor Technology, South Windsor, CT). The ion signal could also be collected using a mass spectrometer.

In Fig. 2A, we show the experimentally observed high harmonics, from orders 15 to 23, as a function of pump-probe time delay. Lower-order harmonics were not observed because of absorption by the $0.2\text{-}\mu\text{m}$ -thick aluminum filter that was used to reject the pump laser light. Even in the raw data, a time-dependent oscillation of the harmonic yield is apparent. For all the harmonic orders observed, the time dependence of the HHG emission (Fig. 2C) shows several common characteristics: a sudden drop in HHG yield when the sample is initially excited at time-zero followed by strong oscillations in the HHG yield imposed on a slowly rising baseline. The strong suppression of harmonic generation at time zero is a result of coherent effects due to the overlap of the pump and probe. Strong oscillations in the harmonic yield are present for both parallel and perpendicular polarizations of the pump and probe (Fig. 2).

Harmonic modulation by the N-N stretch.

The origin of the strong oscillations in the harmonic yield becomes apparent if we apply a discrete Fourier transform to these data. A single peak at $255 \pm 10 \text{ cm}^{-1}$ appears in the transform spectra (Fig. 2, C and D, insets). This frequency corresponds unambiguously to the Raman active 265 cm^{-1} N-N stretch mode of N_2O_4 . Given the ISRS pump mechanism employed here, the initial motion of the vibrational wave packet will be repulsive, with the outer turning point occurring one quarter period after the pump pulse. To verify the exact timing of the emission, we used argon gas in the same setup because HHG from argon exhibits a transient only at time zero because of coherent effects. We thus verified that in N_2O_4 , a large peak in HHG yield appears at $170 \pm 10 \text{ fs}$ in very good agreement with the expected value of $T + T/4$ where $T = 130 \text{ fs}$, which is the vibration period of the N-N stretch mode of N_2O_4 . This timing clearly indicates that harmonic yield maximizes at the outer turning point of the N-N stretch vibration. The first peak in emission at $T/4$ ($\sim 35 \text{ fs}$) is less discernible in the data, probably because of a pump-probe overlap that suppresses the signal.

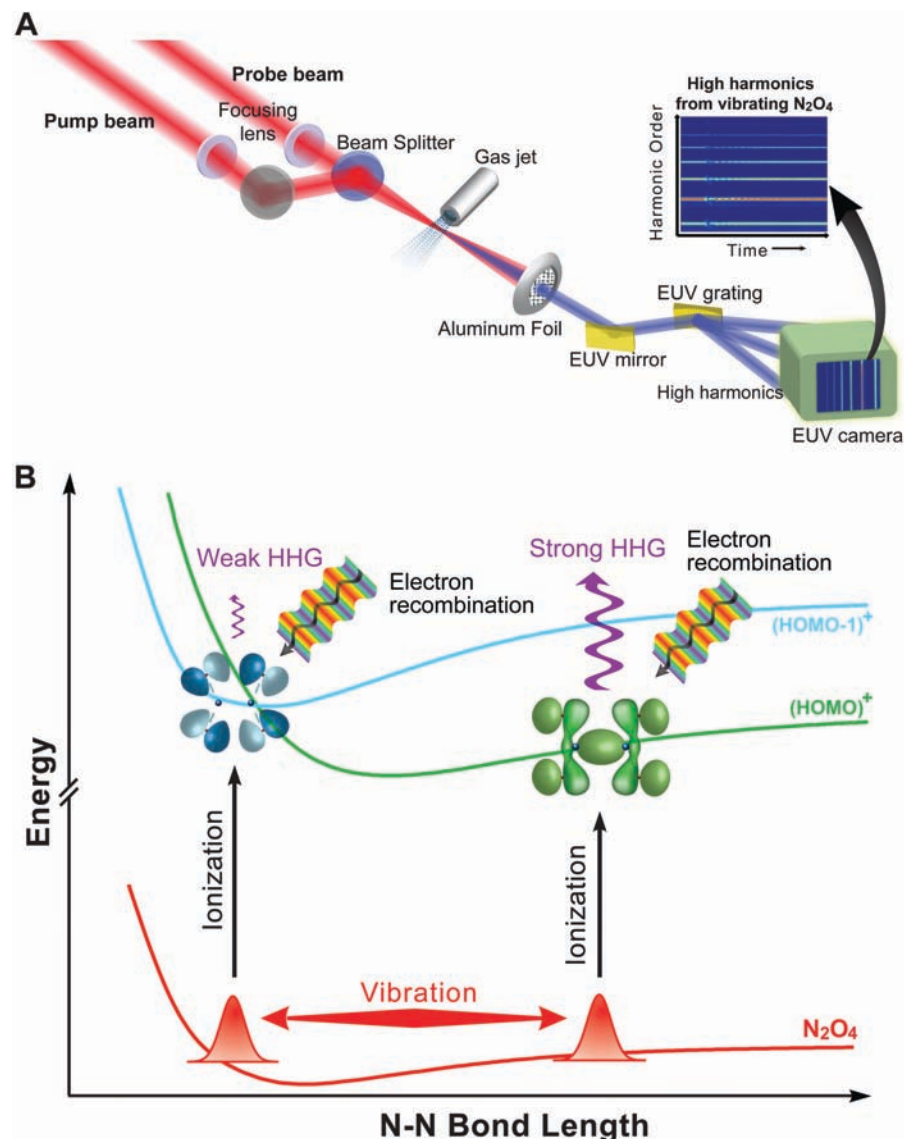


Fig. 1. (A) Experimental setup. N_2O_4 molecules from an effusive nozzle are excited and probed using ultrafast 800-nm laser pulses. The pump-pulse intensity and duration are chosen to impulsively excite, but not ionize or dissociate, N_2O_4 . A more intense collinear probe pulse generates harmonics from the vibrationally excited dimer. (B) Schematic of the experiment.

Only those N_2O_4 molecules for which the N-N bond axis is closely aligned with the pump-beam polarization are vibrationally excited. This same population of molecules is probed by the HHG probe beam, and exhibit oscillations in high harmonic yield corresponding to the N-N stretch as discussed above. In Fig. 2, the amplitude of the harmonic oscillations diminishes as a function of time following the pump pulse, on a time scale consistent with rotational/vibrational dephasing.

We also measured the ionization yield as a function of pump-probe delay (fig. S1). The yield of N_2O_4^+ is approximately the same at the inner and outer turning points. This finding shows that at the inner turning point, the molecule is ionized but harmonic emission is suppressed. Hence, ionization alone (modulation of the ionization

potential or rate due to the vibrational motion) cannot account for the observed large modulation in HHG yield.

The other possibility for the suppression of HHG at the inner turning point of the vibration is a contribution from a different electronic continuum, one that has smaller recombination amplitudes for HHG. We have evidence that this is the case. In Fig. 3, we plot the measured intensity dependence of the HHG peak-to-peak modulation depth of different harmonic orders. The modulation depth increases with increasing laser intensity and decreases with increasing harmonic order. If only a single continuum transition is involved in harmonic emission, then at the relatively high laser intensities that were used in these experiments, ionization will be more saturated at the outer turning point because of

Fig. 2. Harmonic yield as a function of delay between the alignment and HHG pulses using (A) parallel (||) and (B) perpendicular (⊥) pump and probe polarizations. The harmonic yield is normalized to the harmonic emission at negative pump-probe delays. Time dependence of the 17th harmonic yield for (C) parallel and (D) perpendicular polarizations. The insets in (C) and (D) show the Fourier transform, dominated by the N-N stretch mode at 255 cm^{-1} .

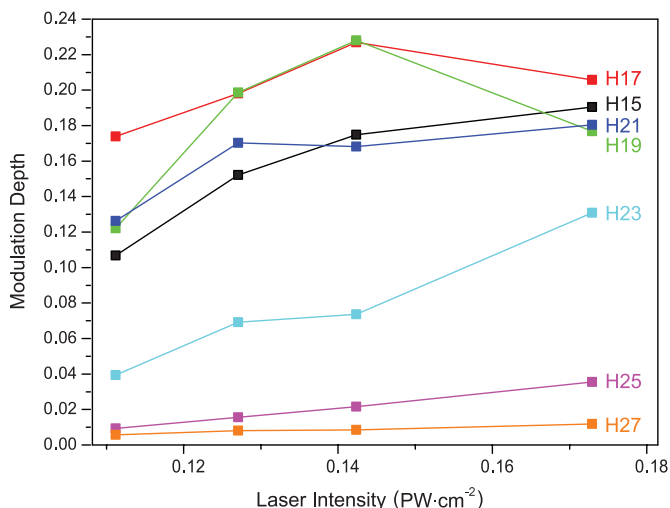
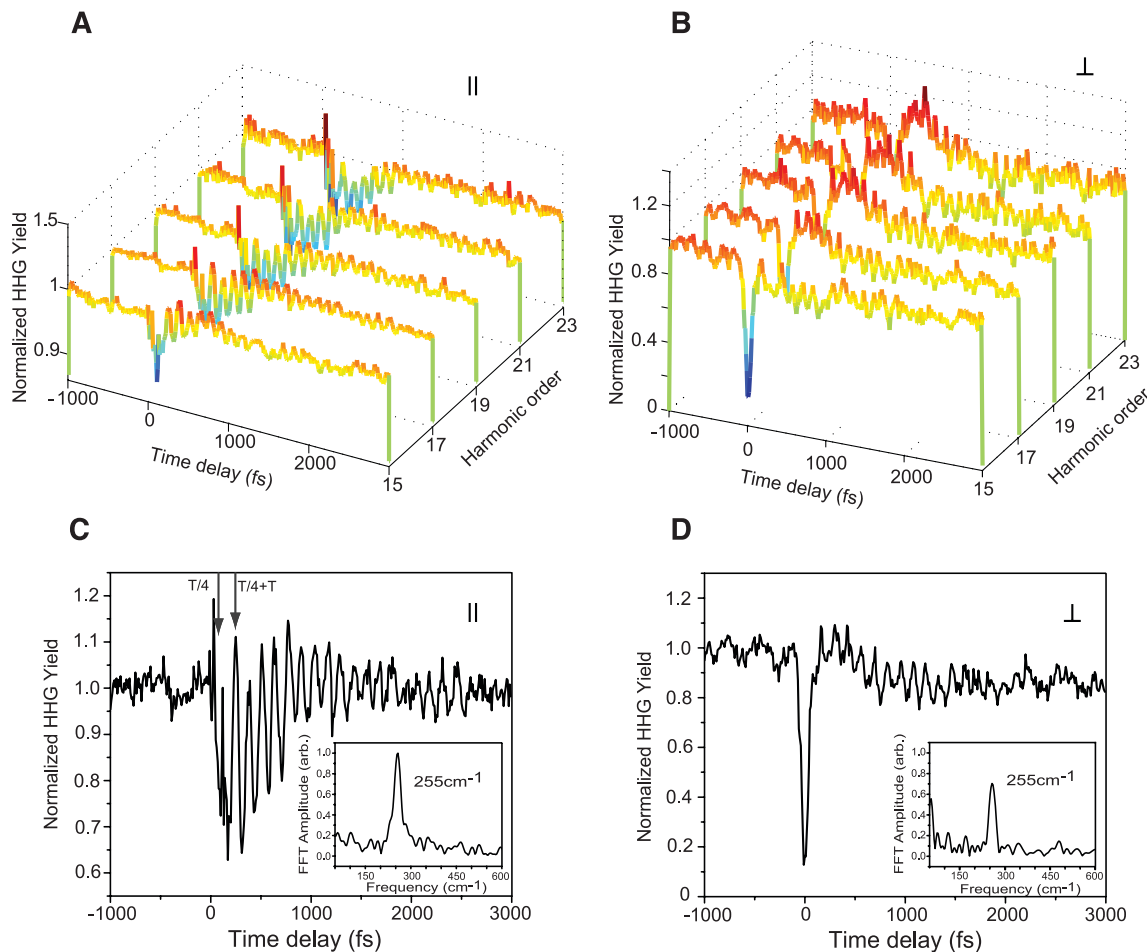


Fig. 3. Laser intensity dependence of the vibrational modulation depth for different harmonic orders, showing an increasing modulation depth with increasing laser intensity.

the lower ionization potential at this position relative to the inner turning point. This should lead to a reduced intensity ratio between harmonics emitted at the outer and inner points of the vibration with increasing laser intensity. In contrast, the observed modulation depth increases with increasing laser intensity.

Ionization of the (HOMO-1) orbital. To understand the effect of a large excursion on the

HHG process, we performed ab initio calculations of the structure of both the N_2O_4 neutral and cation states (25). For N_2O_4 molecules, ISRS in the strongly anharmonic ground-state potential results in large vibrational amplitudes of up to 0.6 \AA (from ~ 1.6 to 2.2 \AA). The calculated potential energy curves for the ground state of neutral N_2O_4 , the ground state of the cation N_2O_4^+ (A_g), and the first excited state of the cation (B_{2g})

are shown in Fig. 4A. The equilibrium bond length of the A_g cation has a substantially elongated N-N bond (2.21 \AA vertical, elongating to 2.25 \AA upon complete optimization). This bond lengthening is a consequence of HOMO ionization to the cation ground electronic state, removing a bonding electron. In contrast, ionization of the (HOMO-1) to the B_{2g} excited state of the cation leaves the N-N bond relatively unchanged (1.75 \AA vertical, increasing to 1.80 \AA upon relaxation). This picture is confirmed by the previously reported He(I) photoelectron spectra of N_2O_4 , which show a delayed onset and long progression to the cation ground electronic state as compared with sharp lines and very limited progression to the cation first excited state (26).

The significant difference in bond length for the ground and excited states of the cation implies a strong bond-length dependence of the structural (Franck-Condon) factors for tunnel ionization: The A_g ground state is expected to be favored at longer N-N distances, whereas the B_{2g} excited channel benefits when the N-N bond is compressed. To quantify this argument, we performed a model calculation of the energy-dependent contribution to the structural ionization factors using the potential energy surfaces shown in Fig. 4A [supporting online material (SOM) text]. The results (Fig. 4B) show that for

Fig. 4. (A) Calculated second-order multiconfigurational quasi-degenerate perturbation theory/complete active space self-consistent field method potential energy curves for neutral N_2O_4 (bottom) and the first two cation states (top). (B) Structural factors for ionization calculated at different bond lengths. At the short bond length, ionization favors the first excited state of the ion (B_{2g} continuum), whereas the ground A_g continuum dominates at long bond lengths

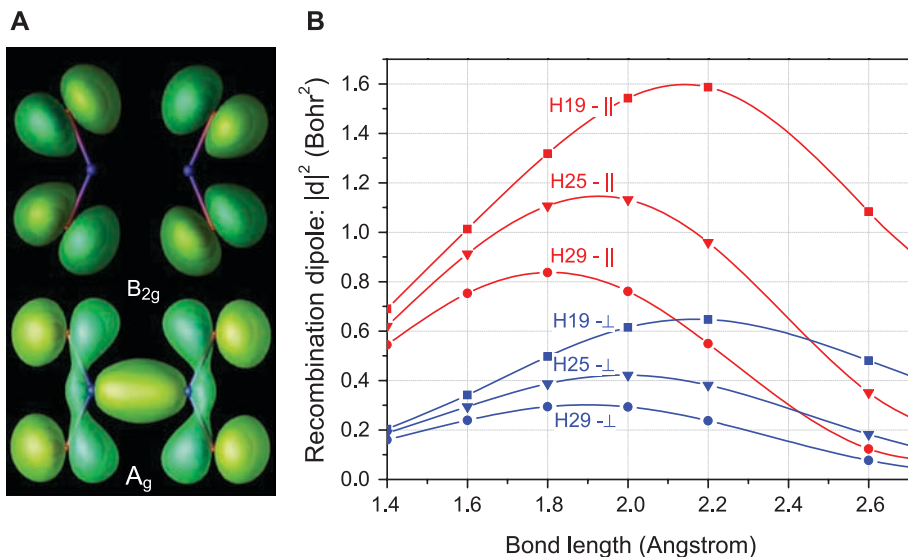
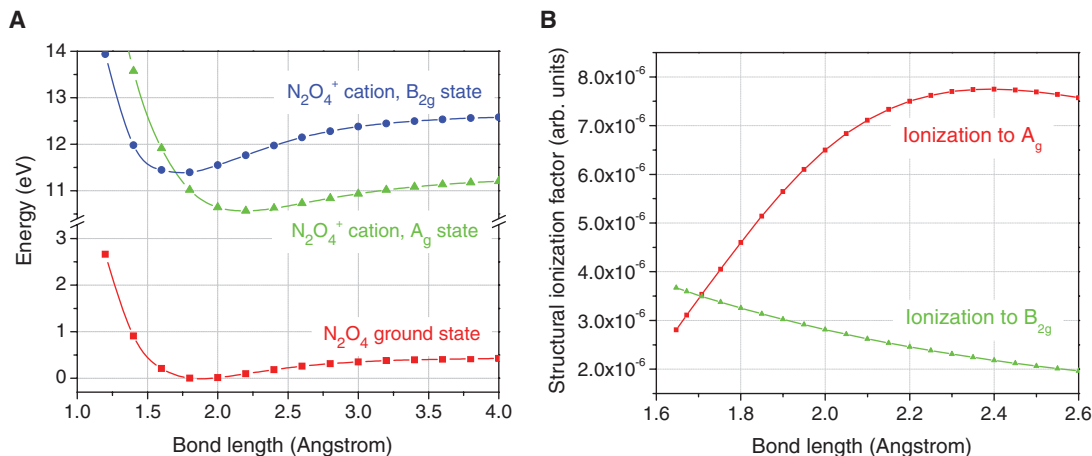


Fig. 5. (A) Dyson orbitals corresponding to ionizing to the A_g cation state and the B_{2g} cation state. The calculated equilibrium bond lengths for the neutral, A_g , and B_{2g} cation states are 1.808 Å [close to the experimental value of 1.756 Å (27)], 2.248 Å, and 1.8 Å, respectively. (B) Recombination dipoles of harmonics for continuum at different bond lengths for parallel (red, ||) and perpendicular (blue, ⊥) pump-probe polarization.

N-N bond lengths ($r_{\text{N-N}}$) below 1.7 Å, structural factors favor ionization to the B_{2g} excited state. At longer bond lengths, ionization to the A_g ground state of the cation is favored, with the corresponding structural factor increasing up to $r_{\text{N-N}} = 2.3$ Å. Thus, because of the contribution of two ionization channels, the ion yield of N_2O_4^+ is not expected to change significantly during the vibration, which is consistent with our experimental findings (fig. S1).

At the relatively high laser intensity used here, saturation due to the depletion of the neutral N_2O_4 population may become an important factor. In this regime, the total number of emitters of each type is determined by the ratio of the ionization rates for each species, rather than by the individual rates. The calculated ratio of the A_g/B_{2g} structural factors in N_2O_4 increases monotonically with $r_{\text{N-N}}$, with the B_{2g} state as the preferred channel at short bond lengths,

whereas the A_g state dominates when the bond is elongated. Thus, the relative importance of the two channels remains the same, even in the presence of saturation. This result is supported by the observed intensity dependence of the HHG modulation depth (Fig. 3), which increases with increasing laser intensity. As discussed earlier, a decreasing modulation depth with laser intensity is expected if only one electronic continuum is contributing to the harmonic signal.

Origins of HHG suppression at the inner turning point. For the propagation of the liberated electron in the continuum, the long-range part of the molecular potential is not substantially influenced by intramolecular vibrations, and no additional modulation of the HHG signal is expected. Therefore, we now consider the electron recombination step. To this end, we calculated the overlap between the N-electron

wave function of the neutral species and the (N-1)-electron wave function of the ion, the Dyson orbital. This calculation captures the change in the electronic structure of the molecule upon electron removal or recombination. Dyson orbitals for the two main ionization channels, calculated at the equilibrium geometry of the neutral species, are shown in Fig. 5A. The final recombination dipoles for the A_g channel as a function of both their N-N bond separations and harmonic order are shown in Fig. 5B. As a result of the presence of nodal planes along all principal directions, the excited ion-state channel (B_{2g}) is suppressed. Nodal planes both decrease recombination matrix elements and reduce the collision probability (11, 12).

The radial dependence of the calculated recombination dipoles \vec{d} is sensitive to the harmonic order. At low harmonic orders (H17 to H21), the matrix elements for the parallel pump-probe orientation increase with the N-N bond length, leading to a doubling in harmonic radiation intensity at $r_{\text{N-N}} = 2.1$ Å ($|\vec{d}_{\text{H19}}|^2 \approx 1.6$ Bohr²) as compared with $r_{\text{N-N}} = 1.5$ Å ($|\vec{d}_{\text{H19}}|^2 \approx 0.84$ Bohr²). At higher orders (H27, H29), the variation of $|\vec{d}|^2$ with the bond length does not exceed 15%. This behavior is consistent with the observed decrease in the modulation of harmonic intensity for higher harmonic orders (Fig. 2A). The lower modulation depth observed for perpendicular polarization of the pump and probe pulse is also consistent with the overall $\approx 60\%$ decrease of the recombination matrix elements for this geometry. For both geometries, the modulation remains in phase for all harmonics, indicating that the observed dependences cannot be explained by the structural dependence of the recombination matrix elements.

Even though the cation excited state (here B_{2g}) does not substantially contribute to HHG emission in N_2O_4 , in other molecules emission from different ionization continua will add coherently; thus, observables such as the ellipticity and phase shift of the HHG emission emerge as sensitive diagnostics of dynamics in polyatomic molecules.

Ruling out NO₂ participation. Because a small portion (<20%) of NO₂ coexists with N₂O₄ in our sample, we had to eliminate the possibility that heterodyne mixing of harmonic emission from N₂O₄ and NO₂ contributed to the observed modulation. If the phase of harmonics emitted from N₂O₄ at the inner turning and outer turning points were different, interference between emissions from NO₂ and N₂O₄ could contribute to the modulation observed. Such phase variations could arise from intrinsic phase changes because of the differing ionization potentials at the inner and outer turning points of the vibration or from different generating ion states; that is, A_g and B_{2g}. Only the latter is consistent with our proposed mechanism. Using an interferometry technique demonstrated recently (20), we monitored the fringe pattern generated by interfering HHG from vibrationally excited and unexcited N₂O₄ molecules (SOM text and fig. S2). No phase change in HHG emission was observed during the vibration within the sensitivity limit of our measurements. This null result is a clear indication that heterodyne mixing does not substantially contribute to our signal.

Outlook. This discovery brings both challenges and opportunities to the application of strong-field ionization and HHG to the study of polyatomic structure and dynamics. Although a simple adiabatic picture involving only a single HOMO orbital may be sufficient for some diatomic molecules, generalization to larger molecules undergoing structural changes (for example, chemical reaction) will require consideration of

both many-body and nonadiabatic electronic dynamics (11, 12). However, the sensitivity of strong-field ionization and HHG to the different ionization continua promises that techniques monitoring tunnel ionization, TRPES, and HHG will uncover detailed information on electronic and nuclear structure and dynamics in polyatomic molecules.

References and Notes

1. A. Stolow, J. G. Underwood, *Adv. Chem. Phys.* **139**, 497 (2008).
2. A. Stolow, A. E. Bragg, D. M. Neumark, *Chem. Rev.* **104**, 1719 (2004).
3. O. Gessner *et al.*, *Science* **311**, 219 (2006).
4. V. Blanchet, M. Z. Zgierski, T. Seideman, A. Stolow, *Nature* **401**, 52 (1999).
5. M. Ferray *et al.*, *J. Phys. At. Mol. Opt. Phys.* **21**, L31 (1988).
6. A. McPherson *et al.*, *J. Opt. Soc. Am. B* **4**, 595 (1987).
7. K. C. Kulander, K. J. Schafer, J. L. Krause, in *Super-Intense Laser-Atom Physics*, B. Piraux, A. L'Huillier, K. Rzazewski, Eds. (Plenum, NY, 1993), vol. 316, pp. 95–110.
8. M. Lewenstein, P. Balcou, M. Y. Ivanov, P. B. Corkum, *Phys. Rev. A* **49**, 2117 (1994).
9. P. B. Corkum, *Phys. Rev. Lett.* **71**, 1994 (1993).
10. H. Kapteyn, O. Cohen, I. Christov, M. Murnane, *Science* **317**, 775 (2007).
11. O. Smirnova, S. Patchkovskii, Y. Mairesse, N. Dudovich, D. Villeneuve, P. Corkum, M. Ivanov, in *11th International Conference on Multiphoton Processes*, J. Anton, B. Martin, R. Moshhammer, J. Ullrich, Eds. (Max-Planck-Institut für Kernphysik, Heidelberg, Germany, 2008), p. 7.
12. Y. Mairesse, O. Smirnova, N. Dudovich, S. Patchkovskii, M. Yu. Ivanov, D. M. Villeneuve, P. B. Corkum, in *11th International Conference on Multiphoton Processes*, J. Anton, B. Martin, R. Moshhammer, J. Ullrich, Eds. (Max-Planck-Institut für Kernphysik, Heidelberg, Germany, 2008), p. Fr62.
13. M. V. Ammosov, N. B. Delone, V. P. Krainov, *Zhur. Eksp. Teor. Fiz.* **91**, 2008 (1986).
14. X. M. Tong, Z. X. Zhao, C. D. Lin, *Phys. Rev. A* **66**, 033402 (2002).
15. M. Lezius, V. Blanchet, M. Y. Ivanov, A. Stolow, *J. Chem. Phys.* **117**, 1575 (2002).
16. M. Smits, C. A. de Lange, A. Stolow, D. M. Rayner, *Phys. Rev. Lett.* **93**, 203402 (2004).
17. S. Patchkovskii, Z. X. Zhao, T. Brabec, D. M. Villeneuve, *J. Chem. Phys.* **126**, 114306 (2007).
18. R. Santra, A. Gordon, *Phys. Rev. Lett.* **96**, 073906 (2006).
19. J. Itatani *et al.*, *Nature* **432**, 867 (2004).
20. X. B. Zhou *et al.*, *Phys. Rev. Lett.* **100**, 073902 (2008).
21. M. Meckel *et al.*, *Science* **320**, 1478 (2008).
22. N. L. Wagner *et al.*, *Proc. Natl. Acad. Sci. U.S.A.* **103**, 13279 (2006).
23. Z. B. Walters, S. Tonzani, C. H. Greene, *J. Phys. At. Mol. Opt. Phys.* **40**, F277 (2007).
24. S. Baker *et al.*, *Science* **312**, 424 (2006).
25. Computational methods are detailed as supporting material on Science Online.
26. T. H. Gan, J. B. Peel, G. D. Willett, *J. Chem. Soc., Faraday Trans. II* **73**, 1459 (1977).
27. A. Kivick, R. K. McMullan, M. D. Newton, *J. Chem. Phys.* **76**, 3754 (1982).
28. The authors thank M. Ivanov and O. Smirnova for helpful discussions. They also gratefully acknowledge support for this work from the U.S. Department of Energy Office of Basic Energy Sciences and the NSF Physics Frontier Centers and the use of facilities from the NSF Engineering Research Center on EUV Science and Technology.

Supporting Online Material

www.sciencemag.org/cgi/content/full/1163077/DC1

SOM Text

Figs. S1 and S2

References

10 July 2008; accepted 24 September 2008

Published online 30 October 2008;

10.1126/science.1163077

Include this information when citing this paper.

The 2.6 Angstrom Crystal Structure of a Human A_{2A} Adenosine Receptor Bound to an Antagonist

Veli-Pekka Jaakola,^{1*} Mark T. Griffith,^{1*} Michael A. Hanson,^{1*} Vadim Cherezov,¹ Ellen Y. T. Chien,¹ J. Robert Lane,² Adriaan P. IJzerman,² Raymond C. Stevens^{1†}

The adenosine class of heterotrimeric guanine nucleotide-binding protein (G protein)-coupled receptors (GPCRs) mediates the important role of extracellular adenosine in many physiological processes and is antagonized by caffeine. We have determined the crystal structure of the human A_{2A} adenosine receptor, in complex with a high-affinity subtype-selective antagonist, ZM241385, to 2.6 angstrom resolution. Four disulfide bridges in the extracellular domain, combined with a subtle repacking of the transmembrane helices relative to the adrenergic and rhodopsin receptor structures, define a pocket distinct from that of other structurally determined GPCRs. The arrangement allows for the binding of the antagonist in an extended conformation, perpendicular to the membrane plane. The binding site highlights an integral role for the extracellular loops, together with the helical core, in ligand recognition by this class of GPCRs and suggests a role for ZM241385 in restricting the movement of a tryptophan residue important in the activation mechanism of the class A receptors.

Extracellular adenosine plays an important role in physiology and initiates most of its effects through the activation of four

guanine nucleotide-binding protein (G protein)-coupled receptor (GPCR) subtypes, A₁, A_{2A}, A_{2B}, and A₃ (1, 2). Each of these four receptors plays

an essential role in responding to adenosine in the central nervous system (3, 4), regulating pain (5), cerebral blood flow (6), basal ganglia functions (7), respiration (8), and sleep (9). These receptor subtypes are primarily coupled to the cyclic adenosine monophosphate (cAMP) second-messenger system, and each has its own unique pharmacological profile. The A_{2A} adenosine subtype is linked to G_s and G_{oif} proteins, and upon receptor activation, the intracellular levels of cAMP increase. At least three of the four adenosine receptor subtypes (A₁, A_{2A}, and A_{2B}) are blocked by naturally occurring methylxanthines, such as caffeine, with modest affinity. It is noteworthy that strong epidemiological evidence suggests that coffee drinkers have a lower risk of Parkinson's disease (10). This effect has been linked to caffeine's interaction with the A_{2A} adenosine receptor, which controls locomotor behavior in basal ganglia, together with dopamine D₂ and metabotropic glutamate

¹Department of Molecular Biology, The Scripps Research Institute, La Jolla, CA 92037 USA. ²Division of Medicinal Chemistry, Leiden/Amsterdam Center for Drug Research, Post Office Box 9502, 2300RA Leiden, Netherlands.

*These authors contributed equally to this work.

†To whom correspondence should be addressed. E-mail: stevens@scripps.edu